

The Effect of Film Thickness and Growth Method on Polyaniline Film Properties

Huyen N. Dinh,**^a Petr Vanýsek,**^b and Viola I. Birss**^{*,z}

Department of Chemistry, University of Calgary, Calgary, Alberta T2N 1N4, Canada

The properties of polyaniline (PANI) films, grown electrochemically on Au using the potential sweep method to two different upper potential limits (type I and II) to various thicknesses in sulfuric acid solution, were studied systematically using cyclic voltammetry, ac impedance, and for the first time, by tracking the rate of the hydrogen evolution reaction (HER). The HER results show that both films follow the nucleation and growth mechanism initially and that continuing growth occurs primarily at the outer PANI surface. Because type II PANI films are formed at a much more rapid rate than type I films, a greater amount of anodic degradation products are incorporated into type II films. Impedance and HER measurements show that type II films, compared for the first time in this work with type I films, have a more open PANI film/Au interfacial structure. A new observation is that the cyclic voltammograms for type I films show a prepeak which is absent for type II films. Furthermore, constant PANI redox peak potentials are observed for type I films, whereas these shift with film thickness for type II films. This unique observation implies that type II films undergo structural changes during their growth, while type I films remain more uniform.

© 1999 The Electrochemical Society. S0013-4651(98)12-003-7. All rights reserved.

Manuscript submitted December 2, 1998; revised manuscript received April 15, 1999.

There has been significant interest in the electrochemical properties of polyaniline (PANI) films on electrode surfaces, largely because of the many promising applications of PANI in electrochromic devices,^{1,2} as supercapacitive materials, as intercalating electrodes in advanced batteries,^{3,4} for electrocatalysis of certain reactions,⁵⁻⁷ in microelectronic devices,⁸ etc.

The properties of PANI films have been extensively studied by many different methods. However, despite the numerous past studies of PANI films, there are still many remaining questions regarding their electrochemical growth mechanism, their structure (particularly at the nanometer scale), and even their electrical properties. Although the impedance technique has been employed quite frequently as a tool for investigating PANI film properties,⁹⁻¹⁷ many of these past studies have focused on the characterization of a single film at different potentials, or of several films of different thickness, but grown by one technique. No single study has been directed at comparing the electrochemical properties of PANI films formed at different rates to different thicknesses at different substrates, etc. As a consequence, there is some uncertainty regarding the dependence of film properties on experimental variables. In fact, many past studies have focused more on the description of the impedance data without much emphasis on interpretation.

Therefore, one of the key objectives of this work was to examine the PANI film impedance response over a wide range of potentials for films formed to various thicknesses while employing several different electrochemical growth conditions on Au and Pt substrates. The principal goal of these studies has been to obtain a better understanding of the growth and structural properties of these films from a careful variation of the experimental parameters within a single controlled study.

In this paper, the electrochemical properties of PANI films, grown by two different methods (type I and type II films) to various thicknesses and studied by cyclic voltammetry (CV) and electrochemical impedance spectroscopy (EIS), are examined systematically. The structural and interfacial properties of the two types of films are compared, for the first time, by tracking the rate of the hydrogen evolution reaction (HER) with time of PANI film growth. It is shown that type II films are more porous, both in the bulk of the film and at

the base of film pores, and are more capacitive than type I films. Type II films also undergo structural changes during film growth, while type I films remain relatively uniform. This work is considered important in terms of providing knowledge regarding how the growth parameters affect PANI film properties and also insight into how to design PANI films with the desired structure, porosity, capacitance, and stability characteristics.

Experimental

Cells and electrodes.—The details of the solutions and the instrumentation used for carrying out CV and ac impedance measurements have been described elsewhere.¹⁸ Standard three-electrode, two-compartment cells were used for PANI growth and ac impedance measurements. The working electrode (WE) was either a polycrystalline Au or Pt wire (Aldrich, 99.99%, 0.5 mm diam), the counter electrode was a large-area Pt gauze, and the reference electrode was a reversible hydrogen electrode (RHE). It should be noted that the Pt WE was used only in the HER experiments. For impedance measurements, a fourth, pseudoreference electrode (a Pt gauze) was placed in the WE compartment and was electrically connected to the RHE via a 6.8 μF capacitor to reduce artifactual phase shifts at high frequencies.¹⁹

All potentials in this paper are reported vs. the RHE, and all current and charge densities are given with respect to the real electrode area. The real area of the Au wire electrode was determined from the Au oxide formation charge, passed to 1.75 V and from comparison with the literature charge density for Au oxide formation (400 $\mu\text{C cm}^{-2}$).²⁰ The real surface area of Pt was established by assuming that a scan between 0.05 and 0.45 V in 1 M H_2SO_4 solution produces one monolayer of adsorbed atomic hydrogen on Pt.²¹ The literature value for the charge of one monolayer of atomic hydrogen on an atomically smooth Pt surface is 220 $\mu\text{C cm}^{-2}$.²¹

Polyaniline growth.—Type I PANI films were grown to various thicknesses on polycrystalline Au wire by cycling at 100 mV s^{-1} for controlled periods of time between 0 and about 1 V in 0.1 M aniline + 1 M H_2SO_4 solution or, for type II films, between 0 and 1.7 V in 0.02 M aniline + 1 M H_2SO_4 solution. The aniline concentration was decreased in order to maintain a reasonable growth rate for type II PANI films, as the higher anodic potential used results in a much higher film growth rate. On Pt, PANI films were grown by cycling between 0.05 and 0.95 V (type I) or 1.7 V (type II). The thicknesses of both types of PANI films were estimated using the relationship of 500 C cm^{-3} . This relationship was determined from our earlier ellipsometry and quartz crystal microbalance (QCM) results for type I films²² and from the anodic type I PANI charge

* Electrochemical Society Student Member.

** Electrochemical Society Active Member.

^a Present address: Los Alamos National Laboratory, Los Alamos, New Mexico 87545, USA.

^b Present address: Department of Chemistry and Biochemistry, Northern Illinois University, DeKalb, Illinois 60115-2862, USA.

^z E-mail: birss@ucalgary.ca

density obtained from slow-sweep CVs between 0 and 0.8 V. These ellipsometry and QCM experiments could not be performed reliably on type II films because of the high degree of surface roughness and optical absorbance of these films. Therefore, it was assumed that type II films have the same charge-to-thickness relationship as type I films. A relationship of 800 C cm^{-3} was reported previously by Rubinstein and Sabatani,²³ Grzeszczuk and Zabinska-Olszak,²⁴ and Deslouis *et al.*,²⁵ but for PANI films grown at constant current and in HCl solutions.

AC impedance measurements.—The PANI-coated Au and Pt WEs were transferred to a fresh, deoxygenated 1 M H₂SO₄ solution to examine the ac impedance response at various potentials, which were changed in both the anodic and cathodic direction. At the start of each batch experiment, the PANI film was equilibrated at 0.1 V in 1 M H₂SO₄ solution for 10 min and then the ac impedance response was measured. The potential was then increased in 50 mV steps, up to 0.60 and then back to 0.1 V, with a 1 min equilibration time at each potential before the ac impedance measurement was started. The data were analyzed using a computer least-squares fit program (EQUIVCRT, B. Boukamp) to establish the equivalent circuit of the system under study.

Results and Discussion

Type I PANI Films Deposited on Au Electrodes

Typical CV behavior.—Type I PANI films were electrodeposited using the most typical conditions used in the literature, *i.e.*, by cycling the potential at 100 mV s^{-1} between 0 and approximately 1 V.²⁶ Films were grown to various thicknesses, and subsequent impedance studies focused on three particular films, which were 55, 80, and 215 nm thick.

Figure 1 shows the CV responses for five films formed on Au in the aniline/sulfuric acid growth solution. The type I PANI growth

process is comparatively slow, requiring about 3 h to form the 215 nm film. Figure 1 shows that the peak potentials, centered at *ca.* 0.4 V, remain essentially constant with increasing film thickness, as indicated by the vertical lines. This could be an indication that PANI retains similar properties regardless of the film thickness. These peaks are associated with the oxidation/reduction of the leucoemeraldine/emeraldine states of PANI. Degradation of PANI is known to occur at $E \leq 1 \text{ V}$,²² and the redox peaks of the degradation products, containing aromatic quinoid groups, are normally seen at *ca.* 0.75 V.²⁷ The soluble forms of the degradation products have been identified as *p*-benzoquinone/hydroquinone, quinone-imines, or oligomers of aniline.²⁸ There is little evidence in Fig. 1 for the presence of decomposition products, consistent with never reaching the degradation potential of $>1 \text{ V}$.

The small prepeak (A_0) centered at 0.25 V has been reported to appear after the film thickness is grown to more than 100 nm.²⁹ Figure 1 shows that the prepeak is well developed for the 145 nm PANI film. Gottesfeld *et al.* suggested that the prepeak is caused by the slow change in film resistivity as it switches from the insulating to the conducting form of PANI.³⁰ However, if this is the case, then it is not clear why the prepeak would be absent altogether for type II films (see the Impedance Analysis section for type II films).

Impedance analysis of type I PANI films.—**General impedance response as a function of potential.**—Figure 2a and b shows a series of Bode and Nyquist plots obtained at potentials from 0.1 to 0.6 V for three PANI films estimated to be 55, 80, and 215 nm thick. It should be noted that the direction in which the potential was changed, *i.e.*, anodically or cathodically, affects the impedance response at any given potential, especially for the insulating and intermediate states of PANI films.^{31,32} Type I PANI films are stable, *i.e.*, the film charge and the impedance response (Bode plots) remain unchanged with time of experimentation, including the use of multiple scans. Potentials greater than 0.6 V were not investigated, as some loss of PANI charge, and hence also of film capacitance, was then observed.

The Nyquist plots (Fig. 2b) show that the PANI film changes from being a much more resistive material at low potentials to a very low-resistance and high-capacitance one at the higher potentials, consistent with numerous previously published works.^{23,33,34} In the fully insulating form of PANI, at 0.1 V, the Nyquist plot (Fig. 2b) shows the presence of essentially only a single semicircle, *i.e.*, only one time constant, with the extrapolated diameter of the circle on the real impedance axis being indicative of a relatively high resistance system. In the conducting form (0.35–0.6 V), the large pseudocapacitance of the film is revealed by the vertical segment in the Nyquist plot, with the extrapolated impedance on the real-axis yielding the very low film (and solution) resistance under these conditions. At potentials between 0.15 and 0.3 V, *i.e.*, in the early segments of the main anodic CV peak (Fig. 1), when the PANI film is neither fully conducting nor fully insulating, the Nyquist plots are more complex, showing an intermediate type of response (see Fig. 2). In fact, the data in this case tend to reflect the presence of several time constants.

From the Nyquist plots it would appear that thinner PANI films are more resistive than thicker ones at 0.1 V, as shown by the larger diameter of the semicircle. As this would be unreasonable, it is possible that the thicker PANI films are not fully reduced at 0.1 V and that some PANI sites are still active, yielding a lower apparent resistance.

For the conducting form of the film, it is notable that at frequencies greater than *ca.* 4 kHz, the impedance becomes inductive in nature, with positive phase angles appearing (Fig. 2a). All impedance experiments involved use of the pseudoreference Pt electrode, and therefore this inductive effect cannot be related to phase shifts due to any lag in the response time of the reference electrode. The appearance of this inductor at high frequencies is believed to arise from electrochemical instrumentation, in general, when high-capacitance, low-resistance systems are under study.³¹ As the inductive response does not originate from the PANI film itself, the high-frequency inductive data were deleted for the detailed analysis of the impedance data.

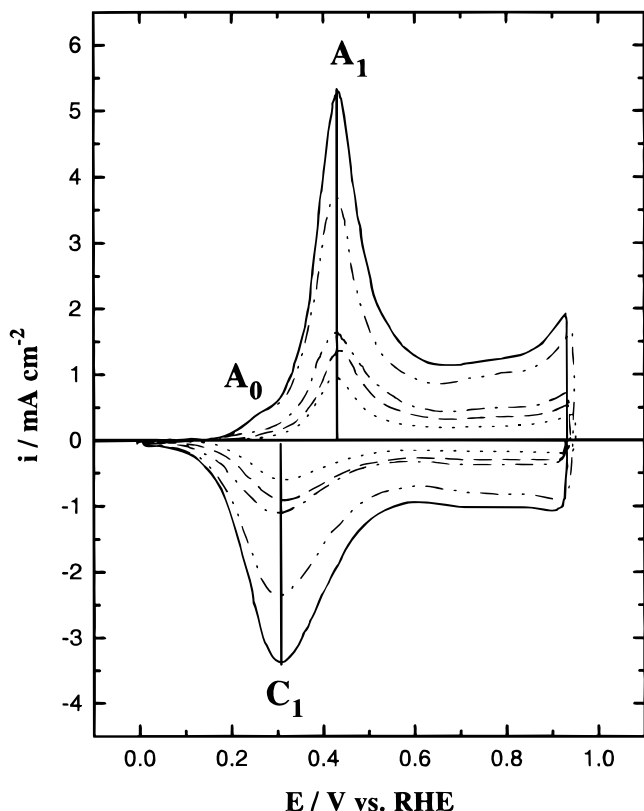


Figure 1. Typical CV response for type I PANI films: (a) 30 nm (••••), (b) 55 nm (---), (c) 80 nm (—•—), (d) 145 nm (—••—), and 215 nm (—), grown on a Au wire in 0.1 M aniline + 1 M H₂SO₄ solution, $s = 100 \text{ mV s}^{-1}$.

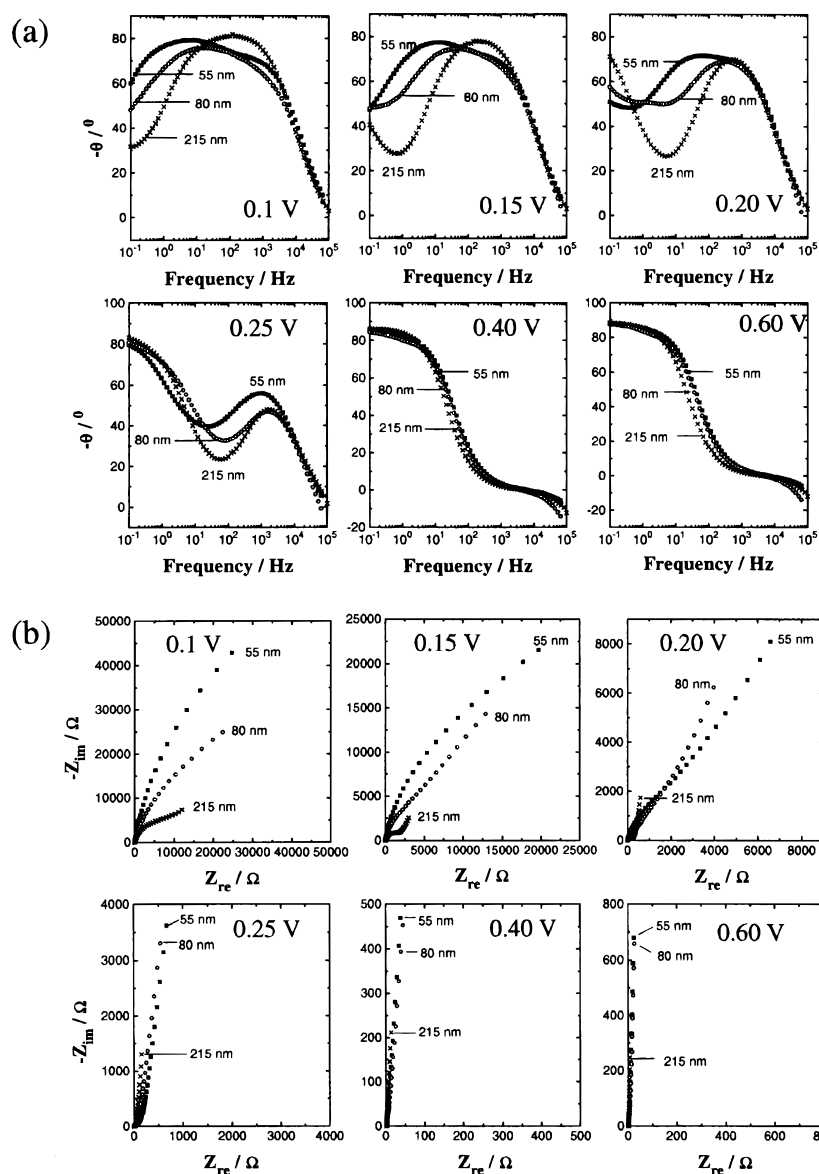


Figure 2. Series of (a) phase-angle Bode and (b) Nyquist plots for type I PANI films on Au in 1 M H_2SO_4 as a function of potential, collected in the anodic direction, and film thickness (■) 55, (○) 80, and (×) 215 nm.

Equivalent circuit approach.—Effect of PANI film thickness and potential.—A relatively common approach to the analysis of imped-

ance data involves the fitting of the data to an equivalent circuit (EC), composed of resistors (R), capacitors (C), and/or constant

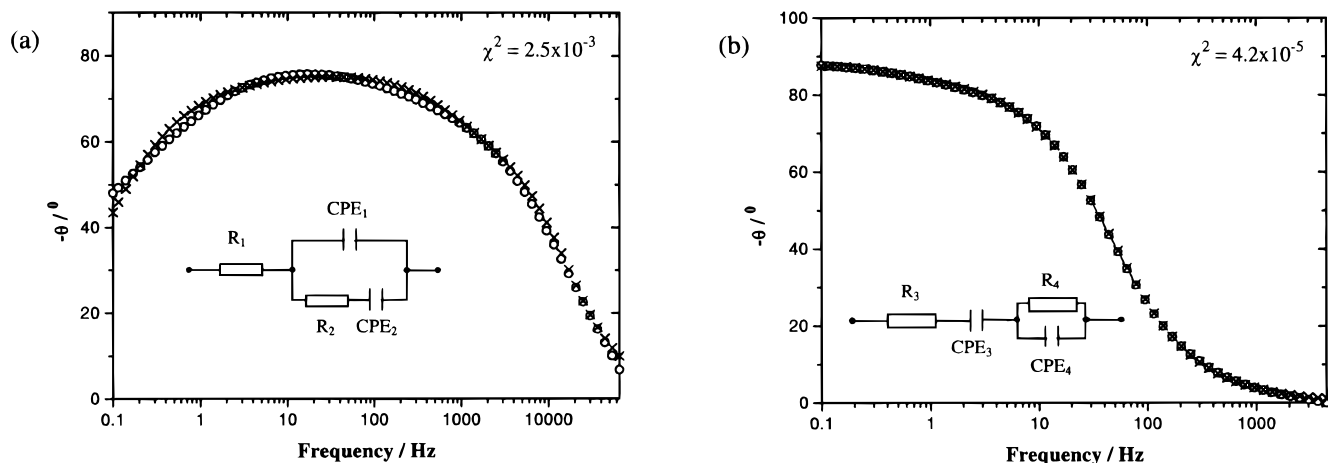


Figure 3. Typical phase-angle Bode plot for an 80 nm (a) reduced, insulating (0.1 Hz to 65 kHz) and (b) oxidized, conducting (0.1 Hz to 4.4 kHz) type I PANI film on Au in 1 M H_2SO_4 at 0.1 and 0.6 V, respectively. Both the experimental data (—○—), collected in the anodic direction, and the corresponding fit (—×—), based on the ECs shown in the figure, are given.

Table I. AC impedance results determined from fitting the data to the circuits shown in Fig. 3 for a 55 nm thick type I PANI film. The EC shown in Fig. 3a was used for PANI films at 0.1-0.25 V. Similarly, the EC shown in Fig. 3b was used for PANI at potentials above 0.25 V.

E (V)	R_1 (Ω)	CPE_1 ($F\text{ cm}^{-2}$)	n_1	R_2 ($\Omega\text{ cm}^2$)	CPE_2 ($F\text{ cm}^{-2}$)	n_2
0.10	2.15	2.00×10^{-5}	0.88	386	2.73×10^{-6}	0.96
0.15	2.07	2.85×10^{-5}	0.85	5.70×10^4	1.53×10^{-4}	0.78
0.20	1.97	3.76×10^{-5}	0.83	4.79×10^3	9.95×10^{-5}	0.61
0.25	1.81	8.93×10^{-5}	0.77	159	2.86×10^{-4}	0.85
E (V)	R_3 (Ω)	CPE_3 ($F\text{ cm}^{-2}$)	n_3	R_4 ($\Omega\text{ cm}^2$)	CPE_4 ($F\text{ cm}^{-2}$)	n_4
0.30	1.61	9.04×10^{-4}	0.97	3.74	2.87×10^{-2}	0.63
0.35	1.55	2.17×10^{-3}	0.95	0.89	7.75×10^{-2}	0.63
0.40	1.54	2.82×10^{-3}	0.95	0.81	8.98×10^{-2}	0.63
0.45	1.54	2.59×10^{-3}	0.96	1.01	9.19×10^{-2}	0.62
0.50	1.53	2.24×10^{-3}	0.97	2.11	9.68×10^{-2}	0.59
0.60	1.54	1.96×10^{-3}	0.99	13.7	6.29×10^{-2}	0.63

phase elements (CPEs). (A CPE is related to a capacitor through the relationship, $C = CPE^n$, where n can assume a value between 0 and 1. When $n = 1$, the CPE is considered to be a pure capacitor.) Numerous efforts^{9-17,23,24,33} have been made to fit data obtained for the conducting and insulating form of a PANI film to either a single, to two, or to even more individual equivalent circuits. Many ECs have been proposed in the literature, particularly for the reduced form of PANI, with some containing up to six circuit elements. A Warburg element has been detected in some cases, especially for very thick PANI films.¹⁷ The circuits suggested for the oxidized form of PANI are much simpler, consisting usually of only a resistance (the solution resistance plus a negligible contribution from the resistance of PANI) in series with a capacitor, reflecting the large pseudocapacitance of oxidized PANI. Attempts to fit data for the intermediate forms of PANI, or all forms of PANI, to a single circuit^{13,14,16} have led to the most complex circuits and data treatment, making it difficult to extract new understanding about PANI properties from these results.

In the present work, it was found that a single EC could not be fitted reliably to the impedance data at all potentials, even for a single PANI film. Therefore, the impedance data for the nonconducting, fully reduced (0.10-0.15 V) and the intermediate forms (0.20-0.30 V) of type I PANI were fitted to the EC shown in Fig. 3a, whereas the impedance data for the oxidized form of the film (0.35-

0.60 V) were fitted to the EC shown in Fig. 3b. The conditions which were the most difficult to fit were for films which were neither fully conducting nor fully insulating, *i.e.*, when measurements were made in the narrow potential range of *ca.* 0.20 to 0.30 V.

Figures 3a and b shows the overlay of the experimental and the fitted data, based on the ECs shown in the same figures, in the form of phase-angle Bode plots for the reduced (0.1 V) and oxidized (0.6 V) 80 nm PANI film, respectively. The fit is good, yielding χ^2 values of 2×10^{-3} and 4×10^{-5} for the reduced and oxidized form of type I PANI, respectively. The phase-angle Bode plots differ when the potential is scanned in the cathodic *vs.* anodic direction (Fig. 3), especially for the insulating and intermediate states of PANI.^{31,32} Therefore, the direction of scan is important and is specified in this paper. Tables I-III (collected in the anodic direction) give the R , CPE , and n values for these two ECs when fitted to the experimental data obtained for the three PANI films (55, 80, and 215 nm) under study. The horizontal double lines on either side of the data obtained at 0.2-0.3 V, seen in Table III, for example, separate the intermediate form of the 215 nm type I PANI film from the conducting and insulating forms.

Considering first the data obtained at the most negative potentials, when type I PANI is fully reduced and electrically nonconducting, CPE_1 is seen to increase with potential. This trend indicates that there may be some mixing of the pseudocapacitance (CPE_2) and CPE_1 . As

Table II. AC impedance results determined from fitting the data to the circuits shown in Fig. 3 for an 80 nm thick type I PANI film. The EC shown in Fig. 3a was used for PANI films at 0.1-0.25 V. Similarly, the EC shown in Fig. 3b was used for PANI at potentials above 0.25 V.

E (V)	R_1 (Ω)	CPE_1 ($F\text{ cm}^{-2}$)	n_1	R_2 ($\Omega\text{ cm}^2$)	CPE_2 ($F\text{ cm}^{-2}$)	n_2
0.10	3.16	3.18×10^{-5}	0.83	5.44×10^4	1.54×10^{-4}	0.61
0.15	2.75	3.36×10^{-5}	0.84	1.01×10^4	7.18×10^{-5}	0.58
0.20	2.48	3.42×10^{-5}	0.85	610	1.64×10^{-4}	0.59
0.25	2.22	9.82×10^{-5}	0.77	47	4.08×10^{-4}	0.87
E (V)	R_3 (Ω)	CPE_3 ($F\text{ cm}^{-2}$)	n_3	R_4 ($\Omega\text{ cm}^2$)	CPE_4 ($F\text{ cm}^{-2}$)	n_4
0.30	1.98	1.23×10^{-3}	0.96	6.22	1.30×10^{-2}	0.78
0.35	1.88	2.77×10^{-3}	0.94	3.46	5.35×10^{-2}	0.72
0.40	1.87	3.58×10^{-3}	0.95	6.55	6.03×10^{-2}	0.71
0.45	1.87	3.27×10^{-3}	0.97	9.55	4.09×10^{-2}	0.73
0.50	1.86	2.79×10^{-3}	0.98	10.7	3.19×10^{-2}	0.73
0.55	1.86	2.53×10^{-3}	0.99	10.1	3.06×10^{-2}	0.73
0.60	1.86	2.47×10^{-3}	0.99	9.69	3.11×10^{-2}	0.73

Table III. AC impedance results determined from fitting the data to the circuits shown in Fig. 3 for a 215 nm thick type I PANI film. The EC shown in Fig. 3a was used for PANI films at 0.1-0.3 V. Similarly, the EC shown in Fig. 3b was used for PANI at potentials above 0.3 V.

E (V)	R_1 (Ω)	CPE_1 ($F\text{ cm}^{-2}$)	n_1	R_2 ($\Omega\text{ cm}^2$)	CPE_2 ($F\text{ cm}^{-2}$)	n_2
0.10	1.90	2.53×10^{-5}	0.92	5.15×10^3	1.40×10^{-4}	0.37
0.15	1.84	3.12×10^{-5}	0.90	1.54×10^3	5.32×10^{-4}	0.63
0.20	1.70	4.98×10^{-5}	0.86	238	9.26×10^{-4}	0.82
0.25	1.46	1.33×10^{-4}	0.78	24	1.25×10^{-3}	0.90
0.30	1.40	1.71×10^{-4}	0.84	1.01	2.25×10^{-3}	0.93
E (V)	R_3 (Ω)	CPE_3 ($F\text{ cm}^{-2}$)	n_3	R_4 ($\Omega\text{ cm}^2$)	CPE_4 ($F\text{ cm}^{-2}$)	n_4
0.35	1.03	7.15×10^{-3}	0.96	0.13	0.10	0.61
0.40	1.01	8.53×10^{-3}	0.97	0.09	0.07	0.86
0.45	1.01	8.09×10^{-3}	0.98	0.12	0.10	0.79
0.50	1.01	7.37×10^{-3}	0.98	0.13	0.10	0.77
0.55	1.01	7.03×10^{-3}	0.98	0.14	0.10	0.77
0.60	1.01	7.33×10^{-3}	0.98	0.15	0.12	0.75

this may be the case, it is appropriate to report CPE_1 at the most negative potential possible, when the contribution from the PANI film reaction (and its pseudocapacitance) is at a minimum. At 0.1 V, CPE_1 has a value of $20\ \mu\text{F cm}^{-2}$ for the 55 nm film, $32\ \mu\text{F cm}^{-2}$ for the 80 nm film, and *ca.* $25\ \mu\text{F cm}^{-2}$ for the thickest (215 nm) film, with associated n values in the range 0.83-0.92 (Tables I-III). In agreement with several suggestions in the prior literature^{10,14,35,36} and based on a comparison with the double-layer capacitance of bare Au, found here to be $55\text{-}60\ \mu\text{F cm}^{-2}$ at these potentials, CPE_1 is considered to reflect the charging of the Au/solution double layer at the base of the pores of the PANI film. Such an interpretation of CPE_1 would be consistent with a structural model of PANI as being a highly porous, solution-accessible material. The primary electrical response, in the case of fully reduced insulating PANI, therefore arises from the underlying Au surface at sites in contact with solution but not blocked by anchoring aniline groups. The n_1 value of 0.83-0.91 would also be consistent with this interpretation, being significantly less than 1, indicative of a capacitive response originating from within or beneath a porous, solution-conducting matrix.³⁷⁻³⁹ It is notable that CPE_1 does not show any particular trend with film thickness, suggesting that the degree of blockage of the Au substrate is essentially constant for type I PANI film, regardless of its thickness.

By comparing these CPE_1 values with that of the double-layer capacitance of the polymer-free Au/solution interface, the fraction of the Au electrode which remains unblocked by the overlying type I PANI film can be estimated to be in the range of 35-55% for these three films. Although this degree of porosity may seem to be quite high, it would be consistent with the high rates of hydrogen evolution achievable at a Pt electrode covered by a PANI film in the insulating state (see the Probing the Metal/Polymer Interface section). PANI films are found to be unaltered electrochemically and no loss of film is seen, despite long times of copious hydrogen evolution, also suggesting a high degree of PANI porosity.

CPE_2 , seen for the reduced form of type I PANI (Fig. 3a) in Tables I-III, may reflect a very small contribution from the PANI pseudocapacitive redox reaction, even at potentials as low as 0.1 V. This is suggested by the observation that its value increases as the potential is increased from 0.1 to 0.3 V, when it takes on a value similar to the film pseudocapacitance obtained using the EC of the conducting film. Furthermore, the low n_2 values suggest that CPE_2 is not a pure capacitance and may reflect the response of the PANI film capacitance distributed within what is mainly an insulating film. It is also notable that CPE_2 is more easily detected at low potentials for the thicker type I PANI films (Fig. 2).

R_2 represents the resistance of the reduced, insulating PANI film at negative potentials. Tables I-III show that R_2 generally decreases

with increasing potential (0.1-0.3 V), as it should, reflecting the increase in PANI film conductivity as it begins to oxidize. R_2 appears to decrease with increasing film thickness, however. For example, at 0.15 V, R_2 is $57\ \text{k}\Omega\text{ cm}^2$ for the 55 nm film, $10\ \text{k}\Omega\text{ cm}^2$ for the 80 nm, and $1.5\ \text{k}\Omega\text{ cm}^2$ for the 215 nm PANI film. As stated previously, it is possible that the thicker PANI films are not fully reduced at 0.1 V, and as some PANI sites are able to oxidize, thick PANI films appear less resistive at these potentials. Finally, the R_1 element reflects the solution resistance between the surface of the PANI film and the RE.

A closer examination of the data in Table III indicates that the resistance of the reduced PANI film, R_2 , is already small at 0.30 V for the 215 nm film. Under these conditions, Fig. 1 shows that only a small fraction of the anodic CV charge has passed. This was confirmed in a separate experiment in which the potential was scanned anodically to 0.35 V, held there for 1 min to simulate the time taken to gather impedance data, and then reversed, reducing the film during the cathodic sweep. Only a very small increase in the cathodic charge is seen vs. that passed in the anodic scan. This confirms that it is sufficient for only a small fraction, *e.g.*, 10% of the PANI film, to be oxidized for a fully conducting response to be seen, as reported previously.^{30,33} A possible explanation is that conducting segments of the film extend from the solution to the underlying metal, thus short-circuiting the film, even while the majority of the film, *ca.* 90% in this case, remains in the reduced and insulating state. This is in agreement with the conclusions of Schultze *et al.*,¹⁰ based on their potential-step experiments.

Considering next the conducting form of type I PANI, the best-fit EC for the data, at essentially all frequencies, is shown in Fig. 3b. It consists of a resistance (R_3) in series with a capacitance (CPE_3) and a R_4 - CPE_4 parallel pair. By dividing the CV current by the sweep rate, the film pseudocapacitance is found to range from 3.5 to $45\ \text{mF cm}^{-2}$, depending on the potential and film thickness. Tables I-III show that the CPE_4 values ($30\text{-}100\ \text{mF cm}^{-2}$) are unreasonably large compared to the *i/s* data and the associated n values are much less than 1, indicating that CPE_4 cannot be the PANI film pseudocapacitance. Because the parallel R_4 - CPE_4 pair is seen only at high frequencies ($>100\ \text{Hz}$ or $>1\ \text{V s}^{-1}$), CPE_4 probably reflects transport limitations within the PANI film and hence, the inability of all sites to react at high frequencies. When the high-frequency data ($>100\ \text{Hz}$) are omitted, the best-fit EC is simply the solution resistance (R_3) in series with the PANI film pseudocapacitance (CPE_3). This simple EC has been reported in the past literature for the conducting form of PANI.²³ It is found to fit well over the frequency range 0.1-100 Hz, and the value of CPE_3 is the same as when the entire frequency range is used (EC in Fig. 3b). A more detailed discussion can be found in Ref. 31 and 32.

In the conducting form of PANI, it is known that the film resistance is negligible, and therefore, R_3 is simply the solution resistance. R_3 remains constant, as it should, at 1.54 Ω for the 55 nm, 1.87 Ω for the 80 nm, and 1.01 Ω for the 215 nm type I PANI films (Tables I-III). The R_3 element varied from one experiment to another, as the position of the WE vs. the RHE varied between experiments, thus causing a variation in the solution resistance. For the same PANI film, the R_3 element was always lower than R_1 . This observation and the fact that R_1 decreases with increasing potential suggest that R_1 includes both the solution resistance and a small contribution from the solution resistance in the pores of the PANI film.

In the conducting form of type I PANI, the underlying Au/solution double-layer capacitance can no longer be detected. This is because the large PANI film pseudocapacitance, CPE_3 , having n_3 values of 0.94-0.99, dominates the electrical response of the conducting PANI film. CPE_3 behaves essentially as a pure capacitor based on its high n_3 values, indicative of the excellent capacitive attributes of conducting PANI films. Figure 4 shows the CPE_3 values as a function of potential for the three type I films under study here. It is seen that the CPE_3 maxima appear at a similar potential as do the CV peak potentials in Fig. 1. Furthermore, the magnitude of the CPE_3 values are similar to the capacitances obtained from slow CV experiments (*i/s*), supporting the assignment of CPE_3 as the film pseudocapacitance. It can be seen, however, that CPE_3 is always less than the film capacitance determined from slow CV experiments (*i/s*). This is consistent with previous reports of the loss of film capacitance in low-voltage-amplitude (ac impedance) experiments vs. that expected from the CVs.^{10,11,17,23,24,33,36,40} The origin of this apparent capacitance loss has been explored by us in another paper.¹⁸

To further validate the assignment and the magnitude of the circuit element CPE_3 , the film capacitance was also extracted from the

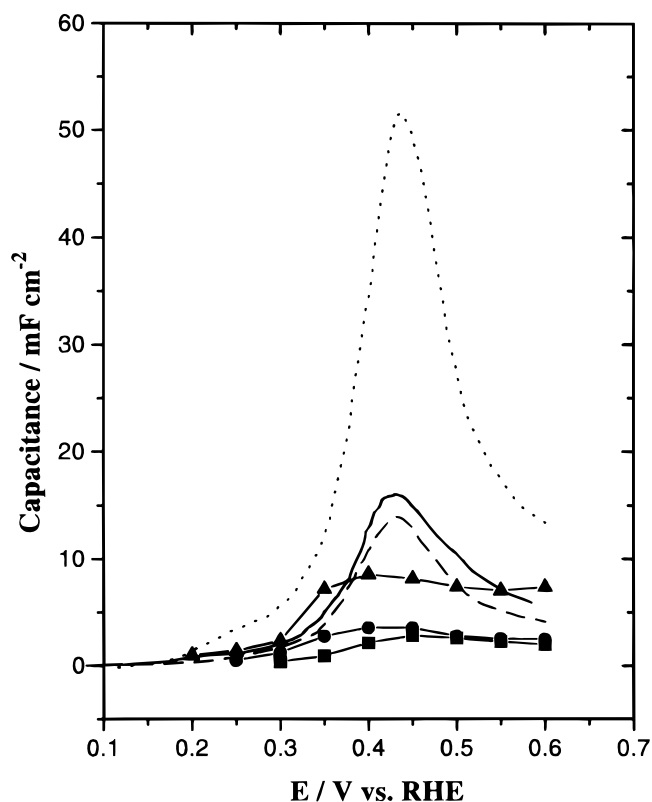


Figure 4. Plots of the CV determined capacitance (*i/s*) vs. potential for a (---) 50, (—) 80, and 215 nm (- - -) type I PANI film on Au in 1 M H₂SO₄. Also shown are plots of CPE_1 (0.2-0.3 V) and CPE_3 (0.35-0.6 V), determined from the ECs in Fig. 3, as a function of potential for three type I PANI films: (—■—) 55, (—●—) 80, and (—▲—) 215 nm. Both CPE_1 and CPE_3 data were obtained in the anodic sweep.

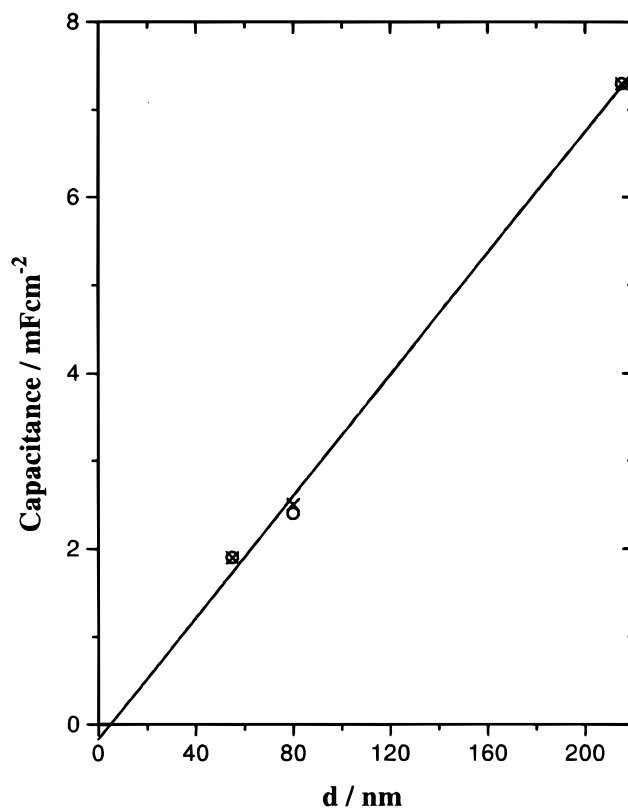


Figure 5. Comparing CPE_3 (×), determined from the EC in Fig. 3b, and the capacitance (○), calculated from the slope of the Z_{im} vs. $\log(f)$ Bode plot ($C = -1/[2\pi(\text{slope})]$), as a function of film thickness for type I, conducting PANI films on Au at 0.6 V in 1 M H₂SO₄. The capacitance was obtained in the anodic sweep.

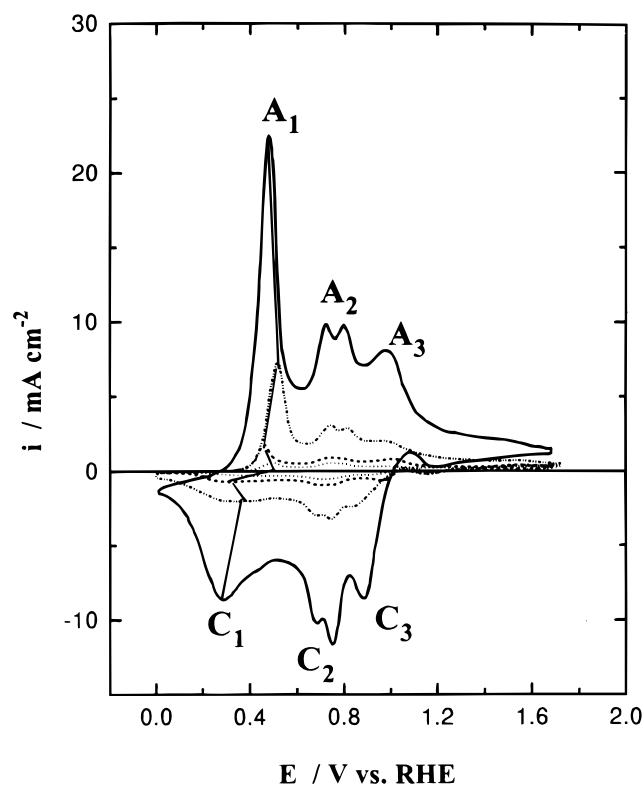


Figure 6. CV responses for type II PANI films: (a) 30 nm (.....), (b) 70 nm (-.-.), (c) 240 nm (---), and (d) 465 nm (—), grown on a Au wire by cycling between 0 and 1.7 V in 0.02 M aniline + 1 M H₂SO₄ solution, 100 mV s⁻¹.

linear slope of the raw Z_{im} data vs. $1/\text{frequency}$ (f) plot (Fig. 5) using the following equation

$$C = \frac{-1}{2\pi f(Z_{im})} \quad [1]$$

The film capacitance calculated in this way correlates very well with the value of CPE_3 determined from the EC approach, as shown in Fig. 5. Furthermore, it is seen that the film capacitance (CPE_3) is linearly related to film thickness, as expected, also validating its assignment.

Type II PANI Films Deposited on Au Electrodes

Typical CV behavior.—Type II PANI films were formed by cycling the potential between 0 and 1.7 V at 100 mV s^{-1} to various final charge densities. Under these conditions, film growth is *ca.* ten times more rapid than for type I films. Higher anodic potentials are expected to increase the rate of diradical dication formation, which would increase the nucleation rate and result in a higher film growth rate.⁴¹⁻⁴³ The PANI-coated Au electrodes were then transferred to aniline-free 1 M H_2SO_4 solution for impedance studies, as for the type I films. Figure 6 shows the CV response for four type II PANI films, estimated as for type I films to be 30, 70, 240, and 465 nm thick. It can be seen that the shapes of the main pair of redox peaks (A_1 and C_1) are somewhat different from those for type I films (cf. Fig. 1). The anodic peak is sharper and the cathodic peak is broader for type II films, resulting in a less symmetrical appearance. Furthermore, type II PANI films yield anodic peak potentials which change with film thickness, even in a single growth sequence. The cathodic peak potential also changes with film thickness so that the difference in peak potential remains constant. Perhaps this change in peak potential is related to a structural change and/or the amount of solvent present within the film⁴⁴ as a function of increasing film thickness.

The most obvious difference in the CVs of Fig. 6 vs. Fig. 1 is the presence of the pair of redox peaks (A_2 and C_2) at *ca.* 0.75 V. Because type II PANI films were grown by cycling to high anodic potentials, some film degradation would have occurred concurrently with PANI film growth. The peaks at 0.75 V have been shown^{26,27,45,46} to be related to the redox reaction of the degradation products, *e.g.*, benzoquinone/hydroquinone (BQ/HQ), quinoneimines, and oligomers of aniline. The third set of redox peaks (A_3 and C_3) centered at *ca.* 1 V reflects the conversion of PANI from the conducting, emeraldine form, to the oxidized, insulating, pernigraniline form, and vice versa. It is this oxidation process, however, which leads to the degradation of PANI and results in the appearance of the BQ/HQ couple. This is because pernigraniline reacts with water to form BQ.⁴⁷ As a result, the appearance of peaks A_1/C_1 is also affected.

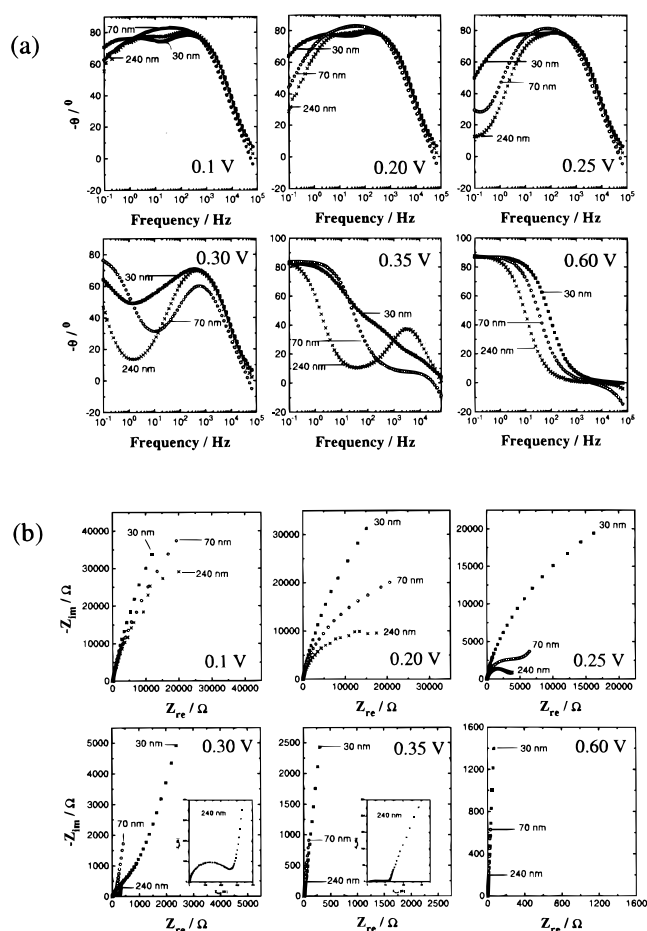


Figure 7. Series of (a) phase-angle Bode and (b) Nyquist plots for type II PANI films on Au, in 1 M H_2SO_4 , as a function of potential, in the anodic direction, and film thickness: (■) 30, (○) 70, and (×) 240. Insets (for 0.30 and 0.35 V) show the Nyquist plots at higher frequencies.

Another difference in the CV response for type II vs. I PANI films is the absence of a pre-peak, even for the thickest film studied here. It is of interest that this observation would argue against the interpretation of the prepeak^{29,30} as arising strictly from the switch in film properties from insulating to conducting in the anodic sweep.

Table IV. AC impedance results determined from fitting the data collected in the anodic direction to the circuits shown in Fig. 8 for a 30 nm thick type II PANI film. The EC shown in Fig. 8a was used for PANI films at 0.1-0.25 V. Similarly, the EC shown in Fig. 8b was used for PANI at potentials above 0.25 V.

E (V)	R_1 (Ω)	R_5 ($\Omega \text{ cm}^2$)	CPE_1 (F cm^{-2})	n_1	R_2 ($\Omega \text{ cm}^2$)	CPE_2 (F cm^{-2})	n_2
0.10	1.07	1.40×10^5	4.51×10^{-5}	0.91	1.21×10^3	1.85×10^{-5}	0.83
0.15	1.08	1.20×10^5	4.49×10^{-5}	0.91	1.27×10^3	1.63×10^{-5}	0.83
0.20	1.08	7.82×10^4	4.81×10^{-5}	0.91	1.40×10^3	1.37×10^{-5}	0.78
0.25	1.07	4.56×10^4	5.51×10^{-5}	0.90	1.15×10^3	2.12×10^{-5}	0.45
E (V)	R_3 (Ω)	R_6 ($\Omega \text{ cm}^2$)	CPE_3 (F cm^{-2})	n_3	R_4 ($\Omega \text{ cm}^2$)	CPE_4 (F cm^{-2})	n_4
0.30	0.99	2.22×10^4	3.95×10^{-4}	0.81	322	1.55×10^{-4}	0.84
0.35	0.95	2.76×10^4	9.95×10^{-4}	0.95	16	7.81×10^{-3}	0.50
0.40	1.04	2.30×10^4	1.57×10^{-3}	0.97	1	6.37×10^{-2}	0.41
0.45	1.06	3.00×10^4	1.79×10^{-3}	0.97	0.21	8.84×10^{-2}	0.49
0.50	1.05	4.30×10^4	1.77×10^{-3}	0.98	0.12	6.93×10^{-2}	0.62
0.55	1.05	5.86×10^4	1.74×10^{-3}	0.97	0.13	1.26×10^{-1}	0.57
0.60	1.05	6.37×10^4	1.76×10^{-3}	0.97	0.12	1.24×10^{-1}	0.58

Table V. AC impedance results determined from fitting the data collected in the anodic direction, to the circuits shown in Fig. 8 for a 70 nm thick type II PANI film. The EC shown in Fig. 8a was used for PANI films at 0.1-0.25 V. Similarly, the EC shown in Fig. 8b was used for PANI at potentials above 0.25 V.

E (V)	R_1 (Ω)	R_5 ($\Omega \text{ cm}^2$)	CPE_1 (F cm^{-2})	n_1	R_2 ($\Omega \text{ cm}^2$)	CPE_2 (F cm^{-2})	n_2
0.10	2.04	1.08×10^5	2.81×10^{-5}	0.93	5.98×10^4	5.51×10^{-6}	0.99
0.15	2.02	8.96×10^4	2.86×10^{-5}	0.93	6.66×10^4	5.65×10^{-6}	0.99
0.20	2.02	4.32×10^4	3.05×10^{-5}	0.93	5.90×10^4	8.08×10^{-6}	0.98
0.25	2.03	1.51×10^4	3.42×10^{-5}	0.92	7.95×10^3	1.44×10^{-4}	0.75
E (V)	R_3 (Ω)	R_6 ($\Omega \text{ cm}^2$)	CPE_3 (F cm^{-2})	n_3	R_4 ($\Omega \text{ cm}^2$)	CPE_4 (F cm^{-2})	n_4
0.30	1.84	5.73×10^{18}	9.5×10^{-4}	0.84	91	1.05×10^{-4}	0.82
0.35	1.80	1.61×10^4	1.77×10^{-3}	0.96	2	1.67×10^{-2}	0.43
0.40	1.81	1.43×10^4	2.48×10^{-3}	0.97	0.17	3.81×10^{-2}	0.77
0.45	1.74	1.98×10^4	2.67×10^{-3}	0.98	0.15	2.45×10^{-2}	0.84
0.50	1.73	2.36×10^4	2.59×10^{-3}	0.98	0.15	2.35×10^{-2}	0.84
0.55	1.73	2.92×10^4	2.54×10^{-3}	0.98	0.16	2.74×10^{-2}	0.82
0.60	1.73	2.94×10^4	2.57×10^{-3}	0.98	0.17	3.20×10^{-2}	0.80

Rather, the absence of a prepeak for type II films would suggest that it represents the oxidation of particular PANI sites or structure, or the presence of a certain reaction stoichiometry present in type I films. It was suggested by our concurrent CV, QCM, and ellipsometry experiments that the prepeak reflects the oxidation of particular PANI sites which are near and/or adjacent to the underlying metal surface.⁴⁴ As type II films are likely to be continuously forming, at least in part, at the metal/polymer interface due to their insulating state at potentials greater than 1.1 V, the conditions must remain unfavorable for the A_0 sites to develop.

The fact that type II PANI films are grown by cycling to high anodic potentials suggests that their growth occurs at both the outer PANI surface, when PANI is conducting (0.4-1 V), and at the underlying metal/solution interface, when PANI is insulating ($E > 1.1$ V). For type I PANI films, on the other hand, film growth occurs when PANI is in its conducting state only, and hence, growth is expected to occur at the PANI/electrolyte interface.

Impedance analysis of type II PANI films.—General impedance response as a function of potential.—As in the case of type I films, impedance data were gathered at potentials between 0.1 and 0.6 V for the three selected type II films. Figure 7a shows a series of phase-

angle Bode plots, obtained as a function of potential, for the three films estimated to be 30, 70, and 240 nm thick. The conversion of the film from insulating to conducting occurs at somewhat more positive potentials, at *ca.* 0.25-0.3 V (Tables IV-VI), compared to what is observed for type I films (0.2-0.25 V) (Tables I-III). The Nyquist plots (Fig. 7b) for type II PANI films otherwise show similar features to Type I films. An inductor-like behavior at above *ca.* 5 kHz is also present for the conducting form of type II films.

EC approach.—Effect of film thickness and potential.—The data for the fully insulating and conducting Type II PANI films were fit to ECs (Fig. 8a and b) which were slightly different from those yielding a best fit for type I PANI (Fig. 3a and b) in that they contain an additional parallel R . This resistance may be related to the leakage current of trace redox reactions. The overall quality of the fits, shown in Fig. 8a and b, was similar to that for type I PANI films.

Tables IV-VI show the fitted values of R , CPE, and n for the three type II PANI films, which can be compared to the data for type I films shown in Tables I-III. Interestingly, the delayed onset of oxidation of these type II PANI films (no prepeak, Fig. 6) provides a wider potential window over which the double-layer capacitance (CPE_1) of the underlying Au/solution interface can be examined for reduced PANI.

Table VI. AC impedance results determined from fitting the data collected in the anodic direction to the circuits shown in Fig. 8 for a 240 nm thick type II PANI film. The EC shown in Fig. 8a was used for PANI films at 0.1-0.25 V and was used to fit data between 0.3 and 0.4 V. Similarly, the EC shown in Fig. 8b was used for PANI at potentials above 0.45 V.

E (V)	R_1 (Ω)	R_5 ($\Omega \text{ cm}^2$)	CPE_1 (F cm^{-2})	n_1	R_2 ($\Omega \text{ cm}^2$)	CPE_2 (F cm^{-2})	n_2
0.10	1.67	3.84×10^4	4.29×10^{-5}	0.92	1.89×10^3	1.26×10^{-5}	0.81
0.15	1.67	2.58×10^4	4.63×10^{-5}	0.92	2.09×10^3	1.05×10^{-5}	0.83
0.20	1.67	1.14×10^4	5.12×10^{-5}	0.91	4.83×10^3	5.68×10^{-6}	0.75
0.25	1.66	2.78×10^3	5.75×10^{-5}	0.90	7.18×10^3	9.68×10^{-5}	0.79
0.30	1.60		8.26×10^{-5}	0.87	161	6.43×10^{-3}	0.79
0.35	1.51		2.07×10^{-4}	0.79	6.54	1.08×10^{-2}	0.95
0.40	1.67		1.38×10^{-2}	0.97	0.50	1.02×10^{-4}	0.90
0.45	1.18		1.40×10^{-2}	0.98	0.49	8.08×10^{-2}	0.17
E (V)	R_3 (Ω)	R_6 ($\Omega \text{ cm}^2$)	CPE_3 (F cm^{-2})	n_3	R_4 ($\Omega \text{ cm}^2$)	CPE_4 (F cm^{-2})	n_4
0.50	1.71	6.63×10^3	1.33×10^{-2}	0.99	0.08	3.61×10^{-1}	0.71
0.55	1.70	7.09×10^3	1.29×10^{-2}	0.99	0.08	3.66×10^{-1}	0.71
0.60	1.70	7.27×10^3	1.31×10^{-2}	0.99	0.08	3.72×10^{-1}	0.71

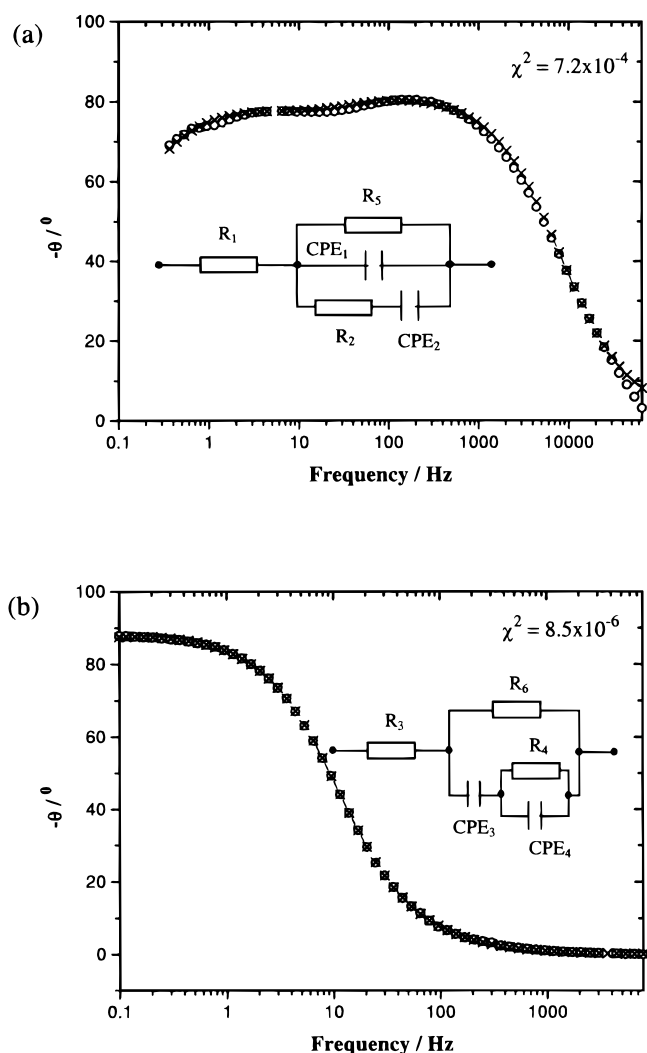


Figure 8. Typical phase-angle Bode plot for the (a) reduced, insulating (0.37 Hz to 65 kHz) and (b) oxidized, conducting forms (0.1 Hz to 7.9 kHz) of PANI (type II, 240 nm) on Au at 0.1 V in 1 M H₂SO₄. Both the experimental data (—○—), collected in the anodic direction, and the corresponding fit (—×—), based on the ECs shown in the figure, are given.

CPE₁ is found to be 46 μF cm⁻² for the 30 nm film, 28 μF cm⁻² for the 70 nm film, and 43 μF cm⁻² for the 240 nm film, with associated *n*₁ values in the range 0.91 to 0.93. The lack of a trend with film thickness is similar to what is seen for type I PANI films. However, the higher fluctuation in CPE₁ with film thickness may suggest that the growth of type II PANI films, which involves scanning to much more positive potentials, a substantially higher growth rate, and the inclusion of decomposition products within the film, also leads to a less predictable film structure. The film porosity, as gauged from the fraction of the Au surface remaining free of anchored aniline groups (from CPE₁), shows no trend with film thickness, although it appears to be larger (50-80%) overall, than for type I PANI films (35-55%). This higher porosity for type II films supported by the results of the HER study (see discussed in the following section) and is consistent with the scanning electron microscopy (SEM) images shown for these films in parallel work.^{32,44}

As was the case for relatively thin type I films, at 0.35 V, the impedance data shows that type II PANI films behave capacitively and are conducting. Thicker type II PANI films appear to become fully conducting at somewhat more positive potentials vs. thin films (see Tables IV-VI), unlike type I PANI films where the thicker films switch on at more negative potentials than the thinner ones. Also, the CVs for type I films show a cathodic shift in the onset of oxidation

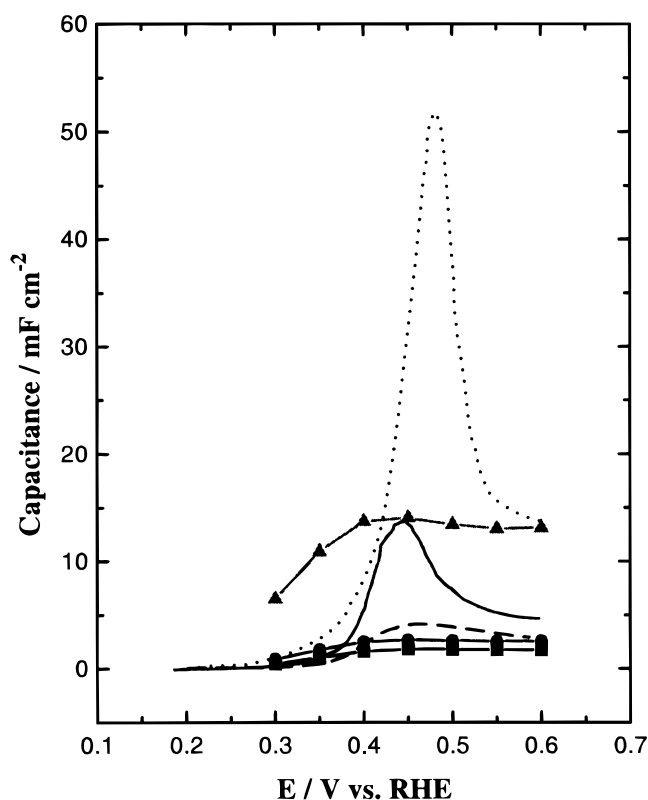


Figure 9. Plots of CV determined capacitance (*i/s*) vs. potential for a (---) 30, (—) 70, and (· · ·) 240 nm type II PANI film in 1 M H₂SO₄. Also shown are plots of CPE₁ (0.3-0.35 V) and CPE₃ (0.4-0.6 V), determined from the ECs in Fig. 8, as a function of potential for three type II PANI films: (—■—) 30, (—●—) 70, and (—▲—) 240 nm. Both CPE₁ and CPE₃ data were gathered in the anodic direction.

with increasing film thickness (Fig. 1), contrary to the case for type II PANI films (Fig. 6).

At 0.40 V and higher, the film resistance becomes very low, and the large PANI film pseudocapacitance, with *n* values of 0.97-0.99, again dominates the electrical response of the film. This film pseudocapacitance (CPE₃) is plotted in Fig. 9 as a function of potential along with the capacitance calculated from the CV response. By comparison with Fig. 4 for type I films, it is seen that a diminished capacitance is again detected in the low-voltage-amplitude impedance experiments, vs. in the CV experiments (*i/s*), for type II PANI films. Compared to type I PANI films, however, this drop is smaller, suggesting that polymer conformational changes, as well as charge compensation by solution ions, may be facilitated by the rapidly grown type II PANI films. Furthermore, the CPE₃ vs. potential plot (Fig. 9) does not exhibit a maximum for type II films as it did for type I films (Fig. 4). Finally, the CPE₃ values are linearly proportional to film thickness (Fig. 10), but the data appear to be more scattered than for type I films.

In summary, type II PANI films are formed at a much rapid rate than are type I films. The consequence of this is a greater extent of incorporation of decomposition products into type II films, along with a more open PANI film/Au interfacial structure, as seen primarily from the larger CPE₁ values for the reduced form of the film. It is also notable that no prepeak is seen, even for very thick type II films.^{32,44} Another interesting difference is in the extent of the decrease of the PANI pseudocapacitance during impedance measurement (CPE₃ for the conducting film) vs. that determined from CV experiments for type II vs. I films.

These differences between type I and II films may originate from the differences in the film structure/porosity of the two films. In parallel work,^{32,44} SEM images have shown that thinner, slowly grown

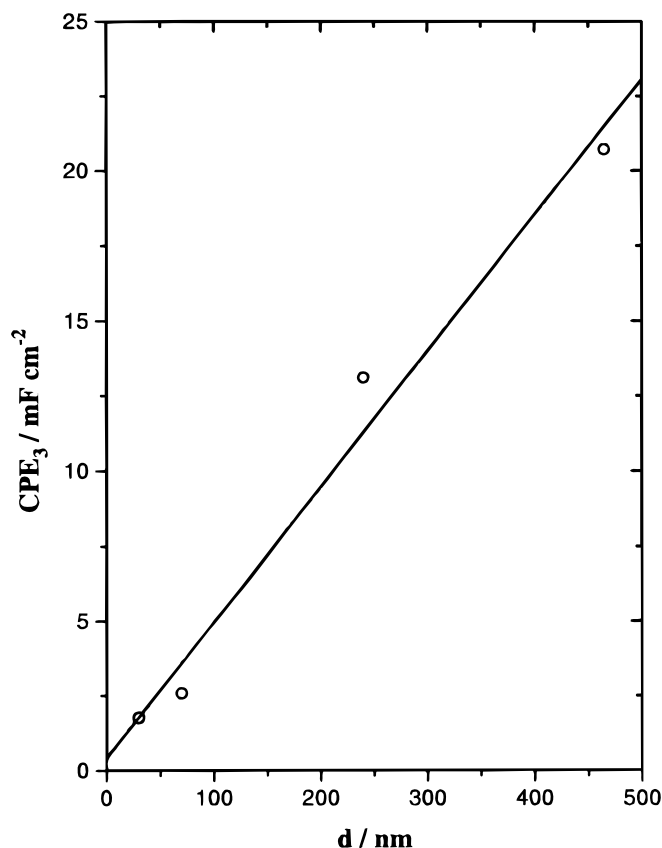


Figure 10. CPE_3 , determined from fitting the EC in Fig. 8b, as a function of film thickness for type II PANI films in 1 M H_2SO_4 at 0.6 V, collected in the anodic scan.

type I PANI films are more globular in nature, whereas the more rapidly grown (and thicker) type II PANI films convert from globular to fibril as a function of film thickness. Impedance and HER results show that type II films are more porous than are type I films. It is therefore possible that type II films undergo structural changes during their growth, while type I films remain more uniform. Type II films contain a greater amount of degradation products, which may lead to structural alterations and may also affect (lower) the film conductivity. It has been suggested^{32,44} that the prepeak may reflect the reaction of PANI sites located near the underlying metal surface. The fact that type II PANI films lack a prepeak suggests that the film structure near the substrate, in particular, is different from that of type I films.

Probing the Metal/Polymer Interface Using HER

The HER technique was employed to probe the fraction of the Pt surface not blocked by polymer for both type I vs. type II PANI films. Because PANI is nonconducting when the HER occurs, the polymer coverage at the metal interface can be determined by assuming that the rate of the HER is proportional to the area of uncovered Pt. It should be noted that only Pt was studied here because the HER on Pt is very facile and its mechanism on Pt has been well studied.

The rate of the HER on bare and PANI-covered Pt was measured in the low-field region, *i.e.*, by scanning the potential from 0 to -50 mV and back at 1 mV s^{-1} , in 1 M H_2SO_4 solution. The solution was agitated by bubbling N_2 at a sufficiently high rate to ensure that the currents were independent of any solution transport processes. After each period of film growth, carried out by cycling the potential between 0.05 and *ca.* 1 V for various time periods the potential was scanned between 0 and 0.6 V until a steady-state CV was obtained, and then the HER data were collected by scanning to -50 mV at 1 mV s^{-1} , as described previously. Similar Tafel slopes (35–40 mV per decade of current) were observed at type II and type I PANI-coat-

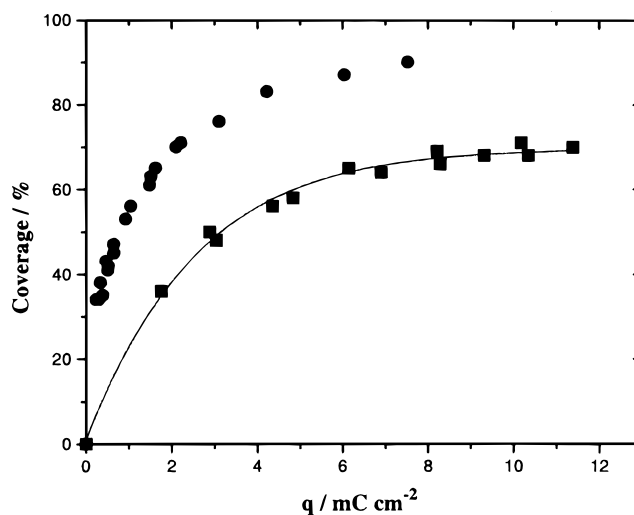


Figure 11. A plot of PANI coverage, as determined from the HER data, vs. charge density, calculated from the CV charge between 0.05 and 0.8 V, during the growth of (●) type I and (■) type II PANI films on Pt in aniline + sulfuric acid solution.

ed Pt, as also seen on bare Pt, indicating that the mechanism for the HER was similar at all electrodes. The fraction of the metal surface covered by PANI was determined from the relative rate (i_0 values) of the HER at 0 V vs. RHE on PANI-coated Pt ($i_{0,PANI/Pt}$) vs. on the bare Pt ($i_{0,Pt}$) electrode in 1 M H_2SO_4 solution, as shown in Eq. 2

$$\text{Coverage} = 1 - \frac{i_{0,PANI/Pt}}{i_{0,Pt}} \quad [2]$$

Figure 11 shows the coverage of PANI, for both type I and II films, as a function of the amount of PANI deposited during growth. It is seen that the coverage of both type I and type II PANI films at the underlying Pt surface increases with the amount of film deposited until a steady-state coverage is reached. This suggests that both type I and type II PANI growths involve an initial nucleation step and then lateral and/or three-dimensional growth of the nucleation centers, resulting in an increase in PANI coverage at later times of growth.⁴⁸⁻⁵² The non-linear dependence of coverage with film thickness, as shown in Fig. 11, is consistent with the prior literature suggestion that the PANI growth mechanism depends on its thickness.^{53,54} During the initial growth phase, nucleation and lateral growth dominate, and hence the coverage at the metal/polymer interface increases. As more film is deposited, the growth of the PANI film is described as one-dimensional needle branching, indicating that growth occurs at the PANI/solution interface, primarily perpendicularly to the PANI surface.^{55,56} Consequently, the metal/polymer interface is barely affected as thicker films are formed, and the coverage by PANI would be expected to reach a relatively constant value at higher charge densities. The coverage data for type II films, as obtained from the rate of the HER, do not show any discontinuities (*e.g.*, peaks), whereas the main PANI peaks (A_1/C_1) shift with film thickness. This suggests that the porosity at the metal/polymer interface is relatively constant, whereas the porosity of the bulk type II film is changing, consistent with the SEM images shown in parallel work.^{32,44}

For the same charge density, PANI coverage is lower for type II vs. type I films (Fig. 11), consistent with the impedance results (CPE_1 values). This may indicate that the growth of type II films is predominantly perpendicular to the metal surface rather than lateral, resulting in lower coverages, a higher porosity, and less protection of the metallic surface. This may be related to the more rapid growth rate of type II vs. I films.

Conclusion

The two different growth methods leading to type I and II PANI films resulted in two electrochemically and structurally different

materials. This is important for the knowledgeable design of PANI film properties for a desired application, e.g., supercapacitors, corrosion protection materials, etc. Although the growth reaction for both films follows the nucleation and growth mechanism, it is interesting that growth of type II films appears to occur at both the outer PANI surface and at the underlying metal/solution interface, whereas growth of type I films occurs at the outer PANI surface only. Furthermore, the high anodic potential used to form type II films results in a higher rate of growth and the formation of larger amounts of degradation products not seen for type I films. EIS and HER studies have revealed, for the first time, that type II films appear to be more porous, both in the bulk part of the film and at the base of pores, and more capacitive compared to type I films. Type I films, however, are more conducting and stable. Type I films would serve as better corrosion protection materials than type II films due to the higher coverage of type I films observed at the metal/polymer interface.

Type I and II films also exhibit some novel differences in their electrochemical behavior. The CVs for type I films show an anodic prepeak, which is absent for type II films. Constant A_1/C_1 peak potentials are observed for type I films during film growth, while these shift with film thickness during type II film growth. This unique observation may be related to the amount of solvent present within the film as a result of the different film structure/porosity of type I vs. II PANI films.

Acknowledgments

The authors are grateful to the Natural Sciences and Engineering Research Council of Canada (NSERC) for their overall support of this work. H.N.D. also acknowledges scholarship support from NSERC, IODE, Alberta Heritage Foundation, A.S.M. International "Calgary Chapter," and the University of Calgary. P.V. gratefully acknowledges an NSERC Visiting Scientist award to the University of Calgary. The authors also wish to thank Amrita Sarpal for contributions to the HER experiments.

The University of Calgary assisted in meeting the publication costs of this article.

References

1. T. Kobayashi, H. Yaneyama, and H. Tamura, *J. Electroanal. Chem.*, **161**, 419 (1984).
2. L. M. Goldenberg, M. C. Petty, and A. P. Monkman, *J. Electrochem. Soc.*, **141**, 1573 (1994).
3. A. G. MacDiarmid, S.-L. Mu, N. L. Somasiri, and W. Wu, *Mol. Cryst. Liq. Cryst.*, **121**, 187 (1985).
4. C. Barbero, M. C. Miras, B. Schryder, O. Haas, and R. Kotz, *J. Mater. Chem.*, **4**, 1775 (1994).
5. G. Mengoli, M. M. Musiani, G. Zotti, and S. Valcher, *J. Electroanal. Chem.*, **202**, 217 (1986).
6. L. Doubova, G. Mengoli, M. M. Musiani, and S. Valcher, *Electrochim. Acta.*, **34**, 337 (1989).
7. C. Q. Cui and J. Y. Lee, *J. Electroanal. Chem.*, **367**, 205 (1994).
8. E. W. Paul, A. J. Ricco, and M. S. Wrighton, *J. Phys. Chem.*, **89**, 1441 (1985).
9. A. D. Jannakoudakis, P. D. Jannakoudakis, N. Pagalos, and E. Theodoridou, *Electrochim. Acta*, **38**, 1559 (1993).
10. O. Genz, M. M. Lohrengel, and J. W. Schultze, *Electrochim. Acta*, **39**, 179 (1994).
11. G. Sandi and P. Vanysek, *Synth. Met.*, **64**, 1 (1994).
12. B. J. Johnson and S.-M. Park, *J. Electrochem. Soc.*, **143**, 1269 (1996).
13. E. Shimada and K. Tachibana, *J. Electrochem. Soc.*, **142**, 4078 (1995).
14. M. Grzeszczuk and P. Poks, *J. Electroanal. Chem.*, **387**, 79 (1995).
15. K. Aoki and K. Hayashi, *J. Electroanal. Chem.*, **384**, 31 (1995).
16. S. Ye, S. Besner, L. H. Dao, and A. K. Vijh, *J. Electroanal. Chem.*, **381**, 71 (1995).
17. P. Fiordiponti and G. Pistoia, *Electrochim. Acta*, **34**, 215 (1989).
18. H. N. Dinh and V. I. Birss, *J. Electroanal. Chem.*, **443**, 63 (1998).
19. F. Mansfeld, S. Lin, Y. C. Chen, and H. Shih, *J. Electrochem. Soc.*, **135**, 906 (1988).
20. A. A. Michri, A. G. Pshchenichnikov, and R. Kh. Burshtein, *Sov. Electrochem.*, **8**, 351 (1972).
21. M. Breiter, *J. Electroanal. Chem.*, **90**, 425 (1978).
22. H. N. Dinh, J. Ding, S. J. Xia, and V. I. Birss, *J. Electroanal. Chem.*, **459**, 45 (1998).
23. I. Rubinstein and E. Sabatani, *J. Electrochem. Soc.*, **134**, 3078 (1987).
24. M. Grzeszczuk and G. Zabinska-Olszak, *J. Electroanal. Chem.*, **359**, 161 (1993).
25. C. Deslouis, M. M. Musiani, and B. Tribollet, *J. Electroanal. Chem.*, **264**, 57 (1989).
26. A. Efremova, A. Regis, and L. Arsov, *Electrochim. Acta*, **39**, 839 (1994).
27. T. Kobayashi, H. Yoneyama, and H. Tamura, *J. Electroanal. Chem.*, **177**, 293 (1984).
28. Y.-B. Shim, M.-S. Won, and S.-M. Park, *J. Electrochem. Soc.*, **137**, 538 (1990).
29. S. Gottesfeld and A. Redondo, *J. Electrochem. Soc.*, **134**, 271 (1987).
30. S. Gottesfeld, A. Redondo, I. Rubinstein, and S. W. Feldberg, *J. Electroanal. Chem.*, **265**, 15 (1989).
31. H. N. Dinh, P. Vanysek, and V. I. Birss, *Electrochim. Acta*, In preparation.
32. H. N. Dinh, Ph.D. Dissertation, The University of Calgary, Calgary, Alberta, Canada (1998).
33. P. M. McManus, R. J. Cushman, and S. C. Yang, *J. Phys. Chem.*, **91**, 744 (1987).
34. T. Komura, H. Sakabayashi, and K. Takahashi, *Bull. Chem. Soc. Jpn.*, **68**, 476 (1995).
35. S. H. Glarum and J. H. Marshall, *J. Electrochem. Soc.*, **134**, 142 (1987).
36. G. Inzelt, G. Láng, V. Kertész, and J. Bácskai, *Electrochim. Acta*, **38**, 2503 (1993).
37. *Impedance Spectroscopy*, J. R. Macdonald, Editor, John Wiley & Sons, New York (1987).
38. J. Hubrecht, M. Embrechts, and W. Bogaerts, *Electrochim. Acta*, **38**, 1867 (1993).
39. W. Yongbin, Y. Renkuan, Y. Hong, and C. Zhonghui, *Synth. Met.*, **55-57**, 1501 (1993).
40. M. Kalaji and L. M. Peter, *J. Chem. Soc., Faraday Trans.*, **87**, 853 (1991).
41. C. M. G. S. Cruz and E. A. Ticianelli, *J. Electroanal. Chem.*, **428**, 185 (1997).
42. J. W. Schultze and A. Thyssen, *Synth. Met.*, **41-43**, 2825 (1991).
43. D. E. Stilwell and S.-M. Park, *J. Electrochem. Soc.*, **135**, 2254 (1988); D. E. Stilwell and S.-M. Park, *J. Electrochem. Soc.*, **135**, 2491 (1988).
44. H. N. Dinh and V. I. Birss, *Electrochim. Acta*, Submitted (1998).
45. W.-S. Huang, B. D. Humphrey, and A. G. MacDiarmid, *J. Chem. Soc., Faraday Trans. 1*, **82**, 2385 (1986).
46. D. E. Stilwell and S.-M. Park, *J. Electrochem. Soc.*, **135**, 2497 (1988).
47. B. Wang, J. Tang, and F. Wang, *Synth. Met.*, **18**, 323 (1987).
48. C. M. G. S. Cruz and E. A. Ticianelli, *J. Electroanal. Chem.*, **428**, 185 (1997).
49. K. Bade, V. Tsakova, and J. W. Schultze, *Electrochim. Acta*, **37**, 2255 (1992).
50. M. E. Vela, G. Andreasen, R. C. Salvarezza, and A. J. Arvia, *J. Chem. Soc., Faraday Trans.*, **92**, 4093 (1996).
51. R. Córdova, M. A. del Valle, A. Arratia, H. Gómez, and R. Schrebler, *J. Electroanal. Chem.*, **377**, 75 (1994).
52. Z. Mandic, L. Duic, and F. Kovacic, *Electrochim. Acta*, **42**, 1389 (1997).
53. S. Mu and J. Kan, *Electrochim. Acta*, **41**, 1593 (1996).
54. B. J. Johnson and S.-M. Park, *J. Electrochem. Soc.*, **143**, 269 (1996).
55. M. E. Vela, G. Andreasen, R. C. Salvarezza, and A. J. Arvia, *J. Chem. Soc., Faraday Trans.*, **92**, 4093 (1996).
56. K. Bade, V. Tsakova, and J. W. Schultze, *Electrochim. Acta*, **37**, 2255 (1992).